

Photoluminescence Tuning in Single-layer MoS₂ via Oxygen Plasma Treatment

Narae Kang^{1,2}, Hari P. Paudel^{1,2}, Michael N. Leuenberger^{1,2,3}, Laurene Tetard^{1,2,*}, and Saiful I. Khondaker^{1,2,4,*}

¹Nanoscience Technology Center (NSTC), ²Department of Physics, ³College of Optics and Photonics (CREOL), ⁴School of Electrical Engineering and Computer Science, University of Central Florida, 12424 Research Parkway, Suite 400, Orlando, Florida, 32826, USA

*To whom correspondence should be addressed. E-mail: laurene.tetard@ucf.edu; saiful@ucf.edu

ABSTRACT

We demonstrate that the photoluminescence (PL) of single-layer molybdenum disulfide (MoS₂) can be significantly tuned by controlled exposure to oxygen plasma. With the variation of the plasma exposure time, the PL changes from a very high intensity to complete quenching accompanied by clear changes in Raman spectra where gradual reduction of MoS₂ peaks were observed along with the appearance of new MoO₃ peaks. Using band structure calculations, we show that the creation of MoO₃ disordered domains upon exposure to oxygen plasma leads to a direct to indirect bandgap transition in single-layer MoS₂ resulting in PL quenching.

Introduction

Fabricating a functional and high performance device made of two-dimensional (2D) materials with controllable atomic scale thickness, has the potential to offer both unique electronic and optoelectronic properties, and to foster important discoveries in the new class of low-dimensional physics.¹⁻³ Due to its exceptional electronic properties, graphene has been the most extensively studied among 2D materials.⁴ However, the inherent lack of bandgap and low absorption of solar photons in pristine graphene greatly limits its use in many electronic and photonic devices. As a result, layered transition metal dichalcogenides (TMDs) and their direct bandgap semiconducting properties in single layers have emerged as great alternatives for 2D device engineering.^{2, 3, 5-7} Molybdenum disulfide (MoS₂), composed of weak van der Waals bonded S-Mo-S units, offers a large intrinsic bandgap, which is strongly dependent on the number of layers: an indirect bandgap (1.2 eV) in bulk MoS₂ transitions to a direct bandgap (1.8 eV) in monolayers.^{6, 7}

The ability to tailor the properties of a material is essential to optimize device functionality. In the case of MoS₂, this can be accomplished not only by controlling the number of layers but also by means of external controls such as chemical doping, strain engineering, irradiation by proton beams or plasma treatment.⁸⁻¹³ In fact, external control becomes the only option for tailoring the properties in single layer device configurations. In case of oxygen plasma, the previous studies focused on multi-layer flakes for controlling the electronic device properties.^{12, 13} Therefore, it is not known whether the optical properties of single layer MoS₂ can be tailored by oxygen plasma. Such knowledge is of great significance from the fundamental point of view as well as for the creation of tailored 2D nanoelectronic and optical devices.

In this paper, we report a systematic study of the effect of plasma exposure on the PL of single-layer MoS₂. By treating the nanosheets via controlled plasma exposure time, we demonstrate the ability to gradually tailor the optical properties of MoS₂ monolayers from high PL response to complete PL quenching. In addition, we monitored incremental changes in Mo-S

bonds and formation of Mo-O bonds as a result of oxygen plasma exposure using Raman spectroscopy. Finally, using band structure calculations, we confirmed that the bandgap of MoS₂ is tuned from direct to indirect in presence of oxygen atoms. The proposed approach to control the PL in single-layer MoS₂ suggests new opportunities to tailor 2D TMDs and of related future electronic/optoelectronic applications.

The measurements were performed on a single-layer MoS₂, which was mechanically exfoliated onto a Si/SiO₂ (250nm) substrate from bulk MoS₂ (SPI Supplies).⁵ The optical and atomic force microscopy (AFM) images of the single-layer MoS₂ are presented in Figure 1 (a) and (b), respectively. The height of the single-layer MoS₂ was estimated at 0.9 nm (Figure 1(b)). Raman spectroscopy (performed on the flake at room temperature using an excitation wavelength at 532 nm) was used to further confirm the number of layers in the MoS₂ flake (Figure 1(c)). The resulting spectrum presents two prominent peaks corresponding to the in-plane E_{2g}¹ and out-of-plane A_{1g} vibration of MoS₂ (Figure 1c inset), and the position difference of these two dominant Raman peaks (Δ) was found to be 19.3 cm⁻¹. This corresponds to the response of a single-layer of MoS₂.^{14, 15} Figure 1(d) shows the PL profile of single-layer MoS₂ with the strong PL peak (peak A1) at 1.84 eV arising from the direct recombination of photo-generated electron-hole pairs with higher luminescence quantum efficiency in the single-layer MoS₂, while the weak shoulder peak (peak B1) at 2.02eV is attributed to the energy split of the valence band spin-orbital coupling of MoS₂ occurring in presence of the SiO₂/Si substrate.⁷

Figure 2 shows the effect of oxygen plasma exposure time on the PL of single-layer MoS₂. The plasma exposure time ranged from 1 to 8 s, with 1 s increments, labeled as t1 to t8 in Figure 2(a). The plasma treatment was carried out using a commercial (Plasma Etch, PE-50) plasma chamber at a power of 100 W operating at 50 kHz. During plasma exposure, the pressure within the plasma chamber was held at 250 – 350 mTorr and a gas mixture of Oxygen (20%) and Argon (80%) flow at a constant rate of 15 sccm. The PL measurements were carried out on a confocal Raman microscope system (Witec alpha300 RA) with a 100 \times objective to reach a spatial resolution of ~300 nm, and a detector with detection range up to ~2.2 eV. To ensure the reproducibility of the data, we followed a careful alignment and optimization protocol. In addition, the laser power was maintained below 1 mW to avoid local heating and additional oxidation of the samples, independently of the integration time required. The integration time was carefully optimized to obtain a satisfactory signal-to-noise ratio while maintaining acceptable data acquisition duration and avoiding drift. For the pristine MoS₂, the intensity of A1 and B1 peak is 31.3 CCD cts and 8.5 CCD cts, respectively as seen in Figure 2(a). The intensity of the PL significantly weakens after t1 exposure and is fully quenched after t3 (Figure 2(a)). Hence by comparing the intensity ratio A1/B1 in the PL spectra as a function of plasma exposure

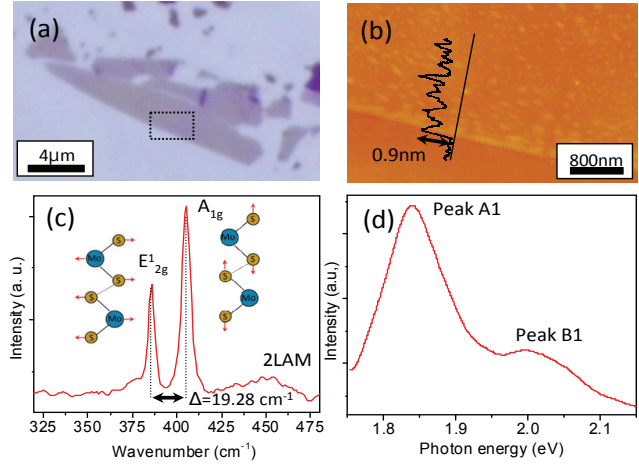


Figure 1 (Color online). Single-layer MoS₂ characterization. (a) Optical, (b) AFM image and height profile, (c) Raman spectrum, (d) photoluminescence (PL) spectrum of exfoliated single-layer MoS₂ on Si/SiO₂ substrate.

time, we show in Figure 2(b) that the highest PL ratio, with a value of 3.7, was observed in pristine single-layer MoS₂, and gradually decreased to 2.3 and 2.1, at t1 and t2, respectively. After t3, we observed the full quenching of PL (represented as a ratio of 1 in the graph). Emitted radiation in PL is caused by the radiative recombination in the sample upon photo-excitation. Radiative recombination is the most effective in direct bandgap semiconductors, such as MoS₂, as it only requires one step recombination for the electron to transition back to its equilibrium level. We postulate that lattice distortions forming as a result of oxygen plasma treatment strongly impede the electron-hole recombination rate in the defected MoS₂ flake, with transition to an indirect bandgap – after total quenching at t3.

To further investigate the origin of the PL intensity decrease leading to a complete quenching in the flake exposed to oxygen plasma for more than 2s, we performed spatially resolved Raman spectroscopy measurements for all samples (pristine to t8). The results are presented in Figure 3. The intensity of all Raman spectra presented was normalized over the amplitude of the Si peak. Raman signature of the pristine single-layer MoS₂ flake (red curve) and of the plasma-treated monolayer MoS₂ as a function of exposure duration (t1 to t8) are presented in Figure 3(a), showing strong variations in terms of peak amplitude, position (wavenumber), width (FWHM), and several important features stand out. First, we found a drastic change in peak intensities with a three-fold amplitude decrease in A_{1g}, four-fold amplitude decrease in E¹_{2g}, and two-fold amplitude decrease in 2LAM (longitudinal acoustic mode). In addition, noticeable changes in position were observed, showing the position of A_{1g} shifts up to 4 cm⁻¹ (blue shift), and the position of E¹_{2g} shifts up to 10 cm⁻¹ (red shift) when compared to pristine single-layer MoS₂ (Figure 3(b)). Similarly, we found an increasing FWHM of A_{1g} and E¹_{2g}. As illustrated in the inset of Figure 1(c), A_{1g}, the out-of-plane optical vibration mode of S atoms, involves the sulfur (S) atomic vibration in opposite directions along the c axis (i.e. axis perpendicular to the basal plane), while in E¹_{2g}, the in-plane optical vibration mode of the Mo-S bond, the displacement of molybdenum (Mo) and of S atoms occur in opposite directions in the basal plane. As Raman active modes arise from polarization induced in the system as a result of the incident light excitation, the change in Raman signature of MoS₂ is indicative of the lattice dynamics of the system. Therefore, the decrease in amplitude of all MoS₂ bands, together with the softening of the A_{1g} phonon mode, and stiffening of E¹_{2g} phonon mode indicate the loss of the symmetry, and disordering of the lattice possibly due to induction of physical plasma interaction.^{16,17} The

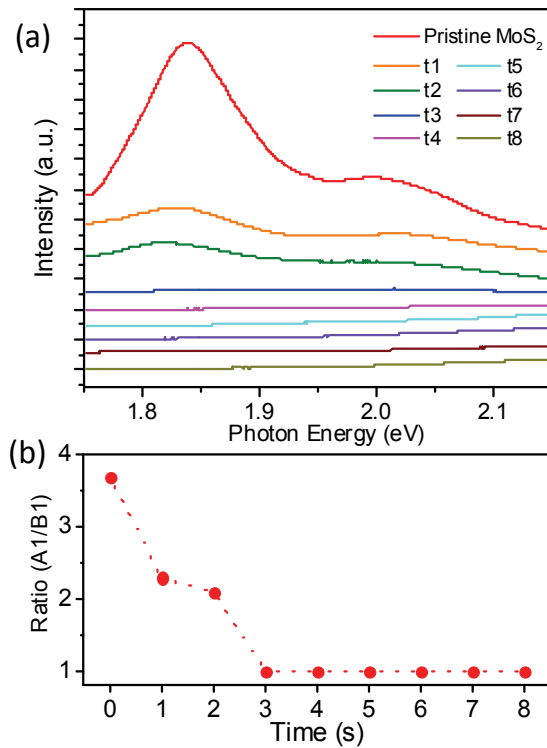


Figure 2 (Color online). (a) Photoluminescence (PL) spectrum of single-layer MoS₂ as function of plasma-treated time. PL spectra of pristine flake shows strong response of the monolayer (red) and gradual PL quenching appears after treatment (t1 to t8). (b) PL intensity ratio (peak A1/peak B1) is plotted with respect to exposure time.

disappearance of the 2LAM mode at 450 cm^{-1} (after t3) also indicates a strong disturbance of the longitudinal acoustic modes in the flake.

Furthermore, we found early signs of Mo-O bonds formation after t2, as can be seen with the appearance of the peak at 225 cm^{-1} in Figure 3, which may help elucidate the disruption of the MoS_2 lattice. The band at 225 cm^{-1} corresponds to the B_{3g} mode of Mo-O in MoO_3 ¹⁸, therefore we hypothesize that vacancies of the S atoms and/or insertion of O atoms in the system occur in the flake during oxygen plasma treatment. Finally, Δ was found to vary from 19 cm^{-1} in pristine MoS_2 to 32 cm^{-1} , which is larger than Δ measured in bulk MoS_2 , signifying major changes in the material's properties.

Our results suggest that during oxygen plasma exposure, energetic O atoms hit the MoS_2 surface and S atoms move out of the lattice site, creating lattice vacancies. This is possible due to the smaller mass of S atoms compared to Mo atoms. Due to the presence of oxygen from the plasma exposure, oxidation takes place at the defect sites created by the S vacancies on the surface, and thus MoO_3 domains are created. In the case of a monolayer of MoS_2 , a change in the surface constitutes a significant change of the entire flake of MoS_2 to localized MoO_3 . The MoO_3 reaction in the MoS_2 processing, interacting with oxygen plasma, can be described as $2\text{MoS}_2 + 7\text{O}_2 \rightarrow 2\text{MoO}_3 + 4\text{SO}_2$.¹⁹ This is in agreement with our hypothesis of a large modification of the bonds should occur inside the flake, transforming from Mo-S only to Mo-S and Mo-O as a result of oxygen exposure. Interestingly, in other reports considering the effect of external control on multi-layer MoS_2 ^{11, 17}, very little effect, if any, was observed in the Raman signature of the treated MoS_2 , indicating low disturbance of the Mo-S bonds in multi-layers flakes. Thus, the results presented here underline the importance of studying the effect of external control on MoS_2 monolayers, and the great impact of oxygen plasma treatment on the material properties of the monolayers.

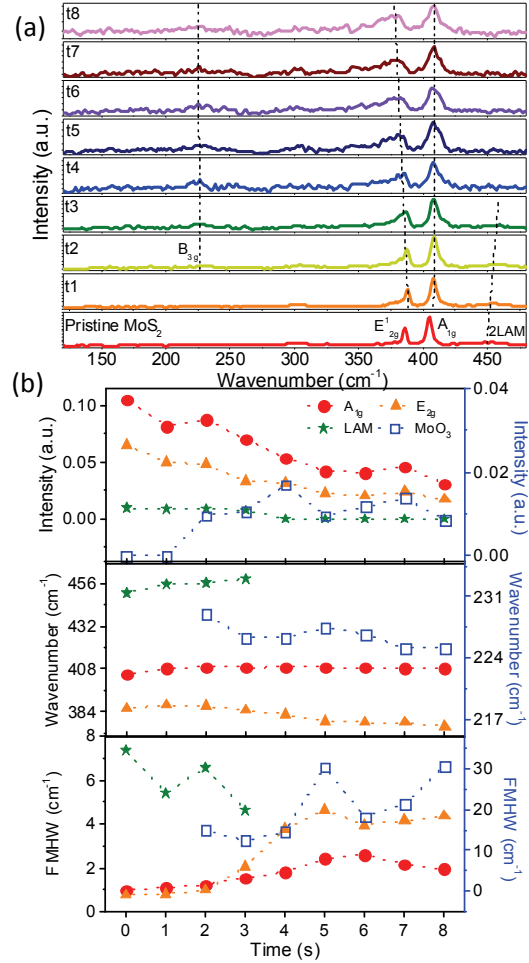


Figure 3 (Color online). (a) Raman spectra of single-layer pristine MoS_2 and plasma-treated MoS_2 as function of plasma exposure time. (b) Summary of normalized peak intensity, wavenumber (position) and FMHW (full-maximum half-width) for A_{1g} (red circle, left-axis), E^1_{2g} (orange triangle, left-axis), 2LAM (green star, left-axis), and MoO_3 (blue open square, right-axis) peak as a function of plasma treatment time.

4

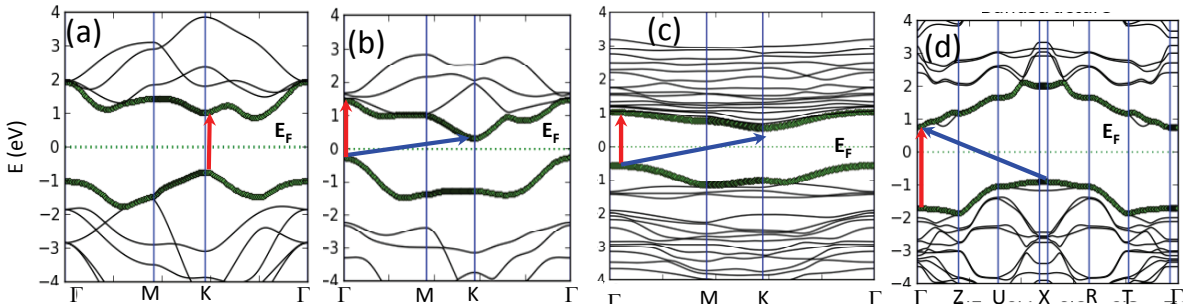


Figure 4 (Color online). Band structure of (a) pristine single-layer MoS₂, (b) single-layer MoS₂ with one S atom replaced by one O atom, (c) single-layer MoS₂ with three S atoms replaced by three O atoms, and (d) a single-layer of MoO₃. Single layer of MoS₂ has direct bandgap at K point (a). The replacement of an S atom by an O atom changes the positions of the band extrema (b,c). The d-bands of MoS₂ at the band extrema are more hole type at the K point (a).

In order to understand the origin of the reduction in PL intensity on oxygen plasma exposure, we performed density functional theory (DFT) calculations to determine the bandstructure of pristine monolayer MoS₂, monolayer MoS₂ with O defects, and monolayer MoS₂ with MoO₃ defects along the high symmetry lines in the first Brillouin zone, as shown in Figure 4. For a pristine single-layer of MoS₂ doped with an O atom, the conduction band minimum (CBM) remains at the K point (as in pristine single-layer MoS₂ (Figure 4(a)) and the valence band maximum (VBM) shifts from the K point to the Γ point, which leads to an indirect gap (blue arrow, Figure 4(b)). Figure 4(c), corresponding to the case where three S atoms are replaced by three O atoms, also shows an indirect bandgap formation (blue arrow) during the oxygen plasma treatment process. Finally, the calculated bandstructure of MoO₃ shows that it is a wide bandgap semiconductor (see Figure 4(d)) with an indirect bandgap. Note that DFT typically underestimates the bandgap, sometimes substantially. Since pristine monolayer MoS₂ has an experimental bandgap of 1.8 eV, and pristine MoO₃ an experimental bandgap larger than 3.2 eV,²⁰ it is plausible to assume that the bandgap of monolayer MoS₂ with MoO₃ defects increases monotonically from 1.8 eV for 0% MoO₃ defect concentration to up to 3.2 eV or higher for 100% MoO₃ defect concentration.^{21, 22} Note also that Kohn-Sham eigenstates resulting from DFT calculations are typically accurate in the sense that they provide an accurate distribution of the electron density and provide accurate results about the type of bandgap.²³ Interestingly, whereas pristine single-layer MoS₂ has a direct bandgap (red arrow), our calculations show that all other configurations have indirect bandgap (blue arrow), which explains the quenching of the PL after oxygen plasma exposure. Therefore, the radiative recombination must be assisted by electron-phonon scattering inside the first Brillouin zone, which leads to the substantial reduction of the PL intensity leading to quenching. In addition, our DFT calculations show that the O defect sites result in a flattening of the 2D monolayer. This means that the bond angle of Mo-S, when measured from the 2D plane, is reduced. Consequently, the in-plane surface of the unit cell increases in the 2D plane, whereas the size of the unit cell in c direction gets smaller. This change in unit cell leads to tensile strain in the 2D plane and compressive strain in c direction. Since the phonon energy spectrum depends on the strain, as e.g. shown for graphene and boron nitride²⁴, we conclude that the energy of the phonon mode E¹_{2g} in the 2D plane decreases, corresponding to a red shift, while the energy of the phonon mode A_{1g} in c direction increases, corresponding to a blue shift. These conclusions agree qualitatively with the red- and blue shifts observed in the Raman spectra shown in Figure 3.

CONCLUSION

In conclusion, we present strong evidence of the ability to tune the photoluminescence of single layer MoS₂ via controlled oxygen plasma exposure. Using Raman spectroscopy, and bandstructure calculation, we show that the band gap of MoS₂ can be engineered from direct to indirect by creating defected MoO₃ domains in the single layer flake with increasing plasma exposure. The physical behavior causing the PL quenching and Raman band shifting is attributed to the lattice distortion engendered by the presence of oxygen in the MoS₂ layer. Our results strengthen the understanding of fundamental physical properties of MoS₂ treated under oxygen plasma, and pave the way toward new possibilities of tailoring two-dimensional transition metal dichalcogenides (TMDs) properties and their related future applications.

ACKLOWDEGEMENT

S.I.K acknowledges financial support from NSF (grant 1102228). M.N.L. acknowledges support from NSF (grant ECCS-0901784), AFOSR (grant FA9550-09-1-0450), and NSF (grant ECCS-1128597).

REFERENCES

- 1 A. K. Geim and I. V. Grigorieva, *Nature* **499**, 419 (2013).
- 2 Q. H. Wang, K. Kalantar-Zadeh, A. Kis, J. N. Coleman, and M. S. Strano, *Nature Nanotechnol.* **7**, 699 (2012).
- 3 V. Nicolosi, M. Chhowalla, M. G. Kanatzidis, M. S. Strano, and J. N. Coleman, *Science* **340**, 1420 (2013).
- 4 V. Singh, D. Joung, L. Zhai, S. Das, S. I. Khondaker, and S. Seal, *Prog. Mater. Sci.* **56**, 1178 (2011).
- 5 B. Radisavljevic, A. Radenovic, J. Brivio, V. Giacometti, and A. Kis, *Nature Nanotechnol.* **6**, 147 (2011).
- 6 K. F. Mak, C. Lee, J. Hone, J. Shan, and T. F. Heinz, *Phys. Rev. Lett.* **105**, 136805 (2010).
- 7 A. Splendiani, L. Sun, Y. Zhang, T. Li, J. Kim, C.-Y. Chim, G. Galli, and F. Wang, *Nano Lett.* **10**, 1271 (2010).
- 8 S. Mouri, Y. Miyauchi, and K. Matsuda, *Nano Lett.* **13**, 5944 (2013).
- 9 K. He, C. Poole, K. F. Mak, and J. Shan, *Nano Lett.* **13**, 2931 (2013).
- 10 A. Castellanos-Gomez, R. Roldan, E. Cappelluti, M. Buscema, F. Guinea, H. S. J. van der Zant, and G. A. Steele, *Nano Lett.* **13**, 5361 (2013).
- 11 T.-Y. Kim, K. Cho, W. Park, J. Park, Y. Song, S. Hong, W.-K. Hong, and T. Lee, *ACS Nano* **8**, 2774 (2014).
- 12 M. Chen, H. Nam, S. Wi, L. Ji, X. Ren, L. Bian, S. Lu, and X. Liang, *Appl. Phys. Lett.* **103**, 142110 (2013).
- 13 M. Chen, H. Nam, S. Wi, G. Priessnitz, I. M. Gunawan, and X. Liang, *ACS Nano* **8**, 4023 (2014).
- 14 C. Lee, H. Yan, L. E. Brus, T. F. Heinz, J. Hone, and S. Ryu, *ACS Nano* **4**, 2695 (2010).
- 15 H. Li, Q. Zhang, C. C. R. Yap, B. K. Tay, T. H. T. Edwin, A. Olivier, and D. Baillargeat, *Adv. Funct. Mater.* **22**, 1385 (2012).

- 16 B. Chakraborty, A. Bera, D. V. S. Muthu, S. Bhowmick, U. V. Waghmare, and A. K. Sood, Phys. Rev. B **85**, 161403(R) (2012).
- 17 J. Yang, S. Kim, W. Choi, S. H. Park, Y. Jung, M.-H. Cho, and H. Kim, ACS Appl. Mater. Interfaces **5**, 4739 (2013).
- 18 M. A. Py, P. E. Schmid, and J. T. Vallin, Nuovo Cimento Della B **38**, 271 (1977).
- 19 B. C. Windom, W. G. Sawyer, and D. W. Hahn, Tribology Lett. **42**, 301 (2011).
- 20 N. M. D. Brown, N. Y. Cui, and A. McKinley, Appl. Surf. Sci. **134**, 11 (1998).
- 21 J. P. Perdew, J. A. Chevary, S. H. Vosko, K. A. Jackson, M. R. Pederson, D. J. Singh, and C. Fiolhais, Phys. Rev. B **46**, 6671 (1992).
- 22 J. P. Perdew, K. Burke, and M. Ernzerhof, Phys. Rev. Lett. **77**, 3865 (1996).
- 23 D. Segev, A. Janotti, and C. G. Van de Walle, Phys. Rev. B **75**, 035201 (2007).
- 24 W. Pan, J. Xiao, J. Zhu, C. Yu, G. Zhang, Z. Ni, K. Watanabe, T. Taniguchi, Y. Shi, X. Wanget, Sci. Rep. **2**, 893 (2012).